Comparing Ultraviolet and Chemical Reduction Techniques for Enhancing Photocatalytic Activity of Silver Oxide/Silver Deposited Nanocrystalline Anatase Titania

ARTICLE *in* THE JOURNAL OF PHYSICAL CHEMISTRY C · APRIL 2009

Impact Factor: 4.77 · DOI: 10.1021/jp8105343

7 AUTHORS, INCLUDING:

Baiju Vijayan
Centre for Materials for Electronics Techno…
43 PUBLICATIONS **1,344** CITATIONS
SEE PROFILE

Satyajit Shukla
National Institute for Interdisciplinary Scie…
81 PUBLICATIONS **1,735** CITATIONS
SEE PROFILE

Biju Silvanose
University of Leuven
29 PUBLICATIONS **942** CITATIONS
SEE PROFILE

MLP Reddy
National Institute for Interdisciplinary Scie…
119 PUBLICATIONS **2,400** CITATIONS
SEE PROFILE

THE JOURNAL OF PHYSICAL CHEMISTRY C

Article

Comparing Ultraviolet and Chemical Reduction Techniques for Enhancing Photocatalytic Activity of Silver Oxide/Silver Deposited Nanocrystalline Anatase Titania

R. Priya, K. V. Baiju, S. Shukla, S. Biju, M. L. P. Reddy, K. Patil, and K. G. K. Warrier

J. Phys. Chem. C, **2009**, 113 (15), 6243-6255• Publication Date (Web): 23 March 2009

Comparing Ultraviolet and Chemical Reduction Techniques for Enhancing Photocatalytic Activity of Silver Oxide/Silver Deposited Nanocrystalline Anatase Titania

R. Priya,[†] K. V. Baiju,[†,||] S. Shukla,[*,†] S. Biju,[‡] M. L. P. Reddy,[‡] K. Patil,[§] and K. G. K. Warrier[†]

Ceramic Technology Department, Materials and Minerals Division (MMD), National Institute for Interdisciplinary Science and Technology (NIIST), Council of Scientific and Industrial Research (CSIR), Industrial Estate P.O., Pappanamcode, Thiruvananthapuram 695 019, Kerala, India, Photochemistry Department, Chemical Sciences and Technology Division (CSTD) NIIST-CSIR, India, and Center for Materials Characterization, National Chemical Laboratory (NCL-CSIR); Pune 411 008, Maharashtra, India

Received: December 1, 2008; Revised Manuscript Received: February 8, 2009

Silver oxide/silver have been deposited, with varying silver concentration (0.01−10 mol %), on the surface of sol−gel derived nanocrystalline anatase titania using two different techniques, namely the ultraviolet reduction and chemical reduction (using stannous ions). The pure and silver oxide/silver-deposited nanocrystalline anatase titania have been characterized for their morphology, average nanocrystallite size, specific surface area, phases involved, surface chemistry, band gap, and photoluminescence using various analytical techniques, such as scanning electron microscopy, transmission electron microscopy, Brunauer, Emmett, and Teller surface-area measurement, X-ray diffraction, X-ray photoelectron spectroscopy, ultraviolet−visible spectrophotometry, and spectrofluorometry, respectively. The photocatalytic activity of pure and silver oxide/silver-deposited nanocrystalline anatase titania has been measured by monitoring the degradation of methylene blue dye in an aqueous solution under ultraviolet-radiation exposure. Within the investigated Ag-concentration range, the maximum photocatalytic activity has been observed for 0.1 and 10 mol % Ag for the chemical-reduction (using stannous ions) and ultraviolet-reduction methods with the corresponding apparent first-order reaction-rate constant (k_{app}) values of 0.228 and 0.151 min^{-1}, which are 3.5 and 2.3 times larger than that of pure nanocrystalline anatase titania (0.065 min^{-1}). The chemical-reduction method (using stannous ions), hence, appears to be more effective than the ultraviolet-reduction method for enhancing the photocatalytic activity of nanocrystalline anatase titania. Various factors such as the surface concentration of superoxide ions, oxygen-ion vacancies, and stannous ions as well as the amount of silver oxide/silver and tin oxide are observed to control the surface-adsorption of methylene blue and photoinduced electron/hole lifetime and, hence, variation in the photocatalytic activity as a function of silver concentration.

Introduction

Nanocrystalline titania (TiO_2) is a semiconductor oxide with a wide band gap of 3.0−3.2 eV having anatase, rutile, and brookite crystal structures. The anatase TiO_2 has been widely investigated for the photocatalytic application for the removal of highly toxic and nonbiodegradable pollutants present in air and wastewater. The mechanism of photocatalysis using the nanocrystalline anatase TiO_2 involves adsorbing the pollutant molecules from air or water on the surface of TiO_2 particles, which are then excited using the ultraviolet (UV) radiation of appropriate energy to generate the electron (e^-) and hole (h^+) pairs within the particle volume. These e^-/h^+ pairs then migrate to the particle surface and serve as redox sites for the destruction of surface-adsorbed pollutants.[1]

It is well-known that the photocatalytic activity of pure nanocrystalline TiO_2, typically with the anatase crystal structure which shows higher photocatalytic activity than the other phases, can be enhanced further by controlling the various material parameters including the average nanocrystallite size, powder morphology, specific surface area, crystallinity, phases involved, dopants, foreign surface oxides, and surface-metal catalysts.[2,3] In the literature, various noble metals such as platinum (Pt),[2−5] gold (Au),[6] palladium (Pd),[7,8] and silver (Ag)[9−26] have been deposited on the surface to improve the photocatalytic activity of nanocrystalline anatase TiO_2. Among these noble surface-metal catalysts, Ag is the cheapest surface activator, and hence, considered here for further investigation.

In the literature,[9−26] Ag-deposited nanocrystalline TiO_2 photocatalyst has been processed using four different techniques, namely the ultraviolet (UV) reduction,[9−19] impregnation and calcination,[20−23] ion-implantation,[24,25] and chemical reduction.[26] Among these methods, the UV-reduction method has been the most popular one, and hence, it has been given further attention in this investigation. On the other hand, there are only few reports, which have utilized the ion-implantation and chemical-reduction methods. As far as the chemical-reduction technique is concerned, we note that this technique using the stannous (Sn^{2+}) ions as reducing agent has not been yet investigated so far in the literature to deposit Ag on the surface of nanocrystalline anatase TiO_2, although this chemical-reduction technique has been well-known for the reduction of palladium (Pd^{2+}) ions

* Corresponding author. Phone: +91-471-2515282. Fax: +91-471-2491712. E-mail: satyajit_shukla@csrrltrd.ren.nic.in.
† MMD, NIIST-CSIR.
‡ CSTD, NIIST-CSIR.
§ NCL-CSIR.
|| Present Address: Catalysis Center, Department of Civil and Environmental Engineering, Northwestern University, Sheridan Road, Evanston, IL 60208.

10.1021/jp8105343 CCC: $40.75
Published on Web 03/23/2009

on the surface of ceramic particles in an electroless metal-coating process.[27,28] As a result, there is no report in the literature dealing with the photocatalytic activity of Ag-deposited nanocrystalline anatase TiO_2 processed via chemical-reduction method using Sn^{2+} ions as reducing agent.

From this point of view, in the present investigation, we modify the surface of sol−gel processed nanocrystalline anatase TiO_2 by depositing Ag with varying concentration via chemical-reduction method (using Sn^{2+} ions) and study its effect on the photocatalytic activity of the former. For comparison, the photocatalytic activity of nanocrystalline anatase TiO_2, surface modified with Ag deposition via UV-reduction method, has also been measured and compared with the new technique. Such systematic analysis, which evaluates and compares the chemical-reduction (using Sn^{2+}-ions) method with the UV-reduction method for enhancing the photocatalytic activity of sol−gel derived nanocrystalline anatase TiO_2, is currently not available in the literature.

Experimental Section

Chemicals. Titanium(IV) isopropoxide ($Ti[OC_3H_7]_4$) and anhydrous 2-propnanol were purchased from Aldrich, India; silver nitrate ($AgNO_3$) from SD. Fine-CHEM Limited, India; Ammonium hydroxide (aqueous NH_4OH, Assay 25−28 wt %) and concentrated HCl (Assay 35 wt %) from Ranbaxy Fine Chemicals Ltd., India; Stannous chloride ($SnCl_2 \cdot 2H_2O$, Assay 97 wt %) from Qualigens Fine Chemicals, India; and methylene blue (MB, AR grade) from Glaxo laboratories Ltd., India. All chemicals were used as received without any further purification.

Sol−Gel Processing of Nanocrystalline Anatase TiO_2. Nanocrystalline anatase TiO_2 was synthesized via conventional sol−gel involving the hydrolysis and condensation of $Ti[OC_3H_7]_4$ in an anhydrous 2-propanol.[29−31] For this purpose, a measured quantity of water was first mixed with 125 mL of anhydrous 2-propanol. A second solution was prepared in which 0.1 M (final concentration) $Ti[OC_3H_7]_4$ was dissolved completely in 125 mL of anhydrous 2-propanol. Both of the solutions were sealed immediately and stirred rapidly using a magnetic stirrer to obtain the homogeneous solutions. The solutions were prepared with the *R* (ratio of molar concentration of water to that of alkoxide-precursor) value of 90. The water part of solution was then added dropwise to the alkoxide part under continuous magnetic stirring. As a result of the hydrolysis and condensation of $Ti[OC_3H_7]_4$ due to the reaction with water, the color of the solution changed from transparent to white. After the complete addition of the water part of the solution to that of the alkoxide part, the resulting suspension was stirred overnight before drying in an oven at 80 °C for the complete removal of solvent and residual water. The dried powder was then calcined at 600 °C for 2 h to crystallize the amorphous TiO_2 completely into the anatase TiO_2.

Processing of Silver Oxide (Ag_2O)/Ag^0 Deposited Nanocrystalline Anatase TiO_2. The sol−gel derived nanocrystalline anatase TiO_2 was then utilized to surface deposit Ag_2O/Ag^0 using two different techniques, namely the UV-reduction and chemical reduction (using Sn^{2+} ions).

UV-Reduction Method. In this technique, 3 g of sol−gel derived nanocrystalline anatase TiO_2 was dispersed in an aqueous $AgNO_3$ solution under continuous magnetic stirring. A proper concentration range of $AgNO_3$ was chosen so as to obtain a Ag/Ti ratio of 10^{-4}, 10^{-3}, 10^{-2}, and 10^{-1}, which corresponds to 0.01, 0.1, 1.0, and 10 mol % Ag, respectively. The pH of solution was adjusted to ∼10−12 by slowly adding an aqueous NH_4OH solution to an aqueous $AgNO_3$ solution containing the nanocrystalline anatase TiO_2 under continuous magnetic stirring. The resulting suspension was then exposed to the UV radiation for 4 h in a Rayonet Photoreactor (The Netherlands) containing 15 W tubes (Philips G15 T8) as the UV source, which emitted the UV radiation having the wavelength within the range of 200−400 nm (corresponding to the photon energy range of 3.07−6.14 eV) peaking at 360 nm. The Ag_2O/Ag^0-deposited nanocrystalline anatase TiO_2 was then separated using a centrifuge (R23, Remi Instruments India Ltd.) and dried in an oven at 80 °C overnight. Change in the color of nanocrystalline anatase TiO_2/Ag composite was noted from white to dark gray with increasing Ag concentration above 0.01 mol %.

Chemical-Reduction (Using Sn^{2+} Ions) Method. In this technique, 3 g of sol−gel derived nanocrystalline anatase TiO_2 was dispersed in 250 mL of acidic aqueous solution containing 10 $g \cdot L^{-1}$ of $SnCl_2$ under continuous magnetic stirring. The pH of solution was adjusted by adding 40 $mL \cdot L^{-1}$ of aqueous HCl solution. The nanocrystalline anatase TiO_2 surface-sensitized with Sn^{2+} ions was then separated using the centrifuge after stirring the suspension for 2 h. The surface-sensitized anatase TiO_2 was dispersed in an aqueous $AgNO_3$ solution under continuous magnetic stirring. Similar to the previous case, a proper concentration range of $AgNO_3$ was chosen so as to obtain the Ag/Ti ratios of 10^{-4}, 10^{-3}, 10^{-2}, and 10^{-1}, which correspond to 0.01, 0.1, 1.0, and 10 mol % Ag, respectively. The pH of the solution was adjusted to ∼10−12 by slowly adding an aqueous NH_4OH solution to an aqueous $AgNO_3$ solution containing the surface-sensitized nanocrystalline anatase TiO_2 under continuous magnetic stirring. The Ag_2O/Ag^0-deposited nanocrystalline anatase TiO_2 was then separated using a centrifuge and dried in an oven at 80 °C overnight. A change in the color of nanocrystalline anatase TiO_2 was noted from white to light gray with increasing Ag concentration.

Characterization of Pure and Ag_2O/Ag^0-Deposited Nanocrystalline Anatase TiO_2. The morphology and average aggregate size (D_{SEM}) of pure and Ag_2O/Ag^0-deposited nanocrystalline anatase TiO_2 were determined using a scanning electron microscope (SEM, JEOL JSM-5600LV, Japan) operated at 15 kV. A transmission electron microscope (TEM, Tecnai G^2, FEI, Netherlands) image of pure nanocrystalline anatase TiO_2 was obtained at 300 kV to analyze the morphology, average nanocrystallite size (D_{TEM}) and its distribution. The selected-area electron diffraction (SAED) pattern was also obtained to confirm the nanocrystallinity and nature of phases involved.

The specific surface area of powders was measured using the Brunauer, Emmett, and Teller (BET) surface-area measurement technique (Micrometrics Gemini 2375 Surface-area Analyzer, U.S.A.) via nitrogen (N_2) adsorption using the multipoint method, after degassing the powders in flowing N_2 at 200 °C for 2 h. The average nanoparticle size (D_{BET}) was calculated using the measured BET surface area via eq 1[31]

$$D_{BET} = \frac{6000}{\rho S} \tag{1}$$

where ρ is the powder density ($g \cdot cm^{-3}$) and *S* the specific surface area ($m^2 \cdot g^{-1}$) measured via BET method.

The crystalline phases present in the pure and Ag_2O/Ag^0-deposited nanocrystalline anatase TiO_2 were determined using the X-ray diffraction (XRD, Phillips, Netherlands). The broad-scan analysis was conducted within the 2θ range of 20−60° using Cu Kα (λ_{Cu} = 1.542 Å) X-radiation.

The surface chemistry of sol−gel derived pure and Ag_2O/Ag^0-deposited nanocrystalline anatase TiO_2 has been revealed using X-ray photoelectron spectroscope (XPS, VG Micro Tech ESCA 3000, United Kingdom) at a base pressure of 10^{-9} Torr using the Mg Kα radiation (1253.6 eV, line width 0.7 eV) generated at a power of 200 W. Both the survey and high-resolution narrow-scan spectra were recorded with the electron pass energy of 50 eV and takeoff angle of 55° to achieve the maximum spectral resolution. Narrow and high-resolution scans were conducted for Sn (3d) and Ag $3d_{5/2}$ to determine the oxidation states of these elements under different processing conditions. The narrow scans were deconvoluted using the peak-fit software (XPSPEAK 41) to reveal the different species of Sn and Ag existing on the surface of nanocrystalline anatase TiO_2. The binding energy (BE) of Au $4f_{7/2}$ at 84.0 ± 0.1 eV was used to calibrate the BE scale of the spectrometer. Any charging shifts produced by the samples were carefully removed using a BE scale referred to C (1s) BE of the hydrocarbon part of the adventitious carbon line at 284.6 eV.[32] Nonlinear least-squares curve fitting was performed using a Gaussian/Lorentzian peak shape after background removal.

The absorption spectra of pure and Ag_2O/Ag^0-deposited nanocrystalline anatase TiO_2 were obtained using a UV−visible (UV−vis) spectrophotometer (UV-2401 PC, Shimadzu, Japan), operated in the diffuse reflectance (DR) mode, for the wavelength within the range of 200−800 nm. The band gap energy (E_{BG}) was calculated using the equation

$$E_{BG} = \frac{hc}{\lambda_{int}} \tag{2}$$

where, h is the Plank's constant (4.135×10^{-15} eV·s), c the velocity of light (3×10^8 m·s^{-1}), and λ_{int} the wavelength (m) corresponding to the intersection of extension of linear part of the spectrum and x axis.

To estimate qualitatively the photoinduced e^-/h^+ lifetime in the pure and Ag_2O/Ag^0-deposited nanocrystalline anatase TiO_2, the room temperature PL spectra were obtained at the excitation wavelength of 327 nm using a Spex-Fluorolog FL22 spectrofluorometer equipped with a double grating 0.22m Spex 1680 monochromator and a 450 W Xe Lamp as the excitation source operating in the front face mode.

Photocatalytic Activity of Pure and Ag_2O/Ag^0-Deposited Nanocrystalline Anatase TiO_2. The photocatalytic activity of pure and Ag_2O/Ag^0-deposited nanocrystalline anatase TiO_2 was studied by monitoring the degradation of MB dye in an aqueous suspension containing the photocatalyst powder under UV-radiation exposure with continuous magnetic stirring. A 75 mL of aqueous suspension was prepared by completely dissolving 0.0072 μmol·L^{-1} of MB dye and then dispersing 0.4 g·L^{-1} of powder in the deionized water. The resulting suspension was equilibrated by stirring in the dark (without the UV-radiation exposure) for 1 h to stabilize the adsorption of MB dye over the photocatalyst powder surface.

The stable aqueous suspension, with continuous magnetic stirring, was then exposed to UV radiation having the wavelength within the range of 200−400 nm peaking at 360 nm using the Rayonet Photoreactor. Following the UV-radiation exposure, a 3 mL sample suspension was taken out of the UV chamber after each 10 min interval for total 1 h of UV-radiation exposure for obtaining the absorption spectra.

The photocatalyst powder was filtered out from the sample suspension using a centrifuge and the filtered solution was examined using a UV−vis spectrophotometer to study the kinetics of degradation of MB dye. The absorption spectrum of MB dye solution was obtained within the range of 200−800 nm as a function of UV-radiation exposure time. The intensity of main absorbance peak (A) of MB dye solution, located at 656 nm, was taken as a measure of residual MB dye concentration (C). The UV−vis absorption spectrum of the MB dye solution, without the addition of photocatalyst powder and UV-radiation exposure, was also recorded (A_0) as a reference spectrum corresponding to the initial MB dye concentration (C_0). The normalized residual MB dye concentration was calculated using the relationship of the form

$$\left(\frac{C}{C_0}\right)_{MB} = \left(\frac{A}{A_0}\right)_{656nm} \tag{3}$$

The absorption spectrum of MB dye solution after stirring the suspension in the dark for 1 h (that is, just before the UV-radiation exposure) was also recorded (A') in order to obtain the concentration of MB dye adsorbed (in percentage) on the surface of photocatalyst powder, using the relationship of the form

$$C^{MB}_{Adsorbed}(\%) = \left[1 - \left(\frac{A'}{A_0}\right)_{656nm}\right] \times 100 \tag{4}$$

A photocatalysis experiment was performed in the absence of photocatalyst powder to confirm the stability of MB dye in an aqueous solution under continuous UV-radiation exposure. Under this condition, the initial MB dye concentration remained unchanged even after irradiating the sample for total 1.5 h.

Results

Morphological, Structural, and Chemical Analysis of Pure and Ag_2O/Ag^0-Deposited Nanocrystalline Anatase TiO_2. Typical SEM and TEM images of sol−gel processed nanocrystalline anatase TiO_2 are presented in Figures 1a and 1b. The nanocrystalline anatase TiO_2 appears to be an agglomerated powder with D_{SEM} of ∼200 nm, Figure 1a. The aggregates are further observed to consist of small nanocrystallites with D_{TEM} of ∼15−30 nm, Figure 1b. The SAED pattern as shown in Figure 1c displays continuous rings confirming the nanocrystalline nature of the powder. The ring pattern has been indexed according to the anatase structure, which validates the formation of nanocrystalline anatase TiO_2 via present sol−gel method.

The N_2 adsorption/desorption isotherms and differential pore volume curve (Barret−Joyner−Halenda (BJH) plot) obtained for the pure nanocrystalline anatase TiO_2 are presented in Figure 2, panels a and b. The isotherms are of type IV and exhibit typical hysteresis behavior of type H3, Figure 2a, which suggests that the sol−gel processed nanocrystalline anatase TiO_2 is a mesoporous powder having an average pore size of ∼15 nm, Figure 2b, and the BET surface area of 28 m^2·g^{-1} with D_{BET} of ∼54 nm estimated using eq 1. No drastic change in the morphology, BET surface area, and pore size distribution is noted after the Ag-deposition using two different techniques.

Typical XRD pattern obtained for the sol−gel derived nanocrystalline TiO_2 is shown in Figure 3. The diffraction pattern has been identified as that of anatase TiO_2 after comparison with the JCPDS card # 21-1272, which is in agreement with the SAED pattern, Figure 1c. The XRD patterns obtained using Ag_2O/Ag^0-deposited nanocrystalline anatase TiO_2

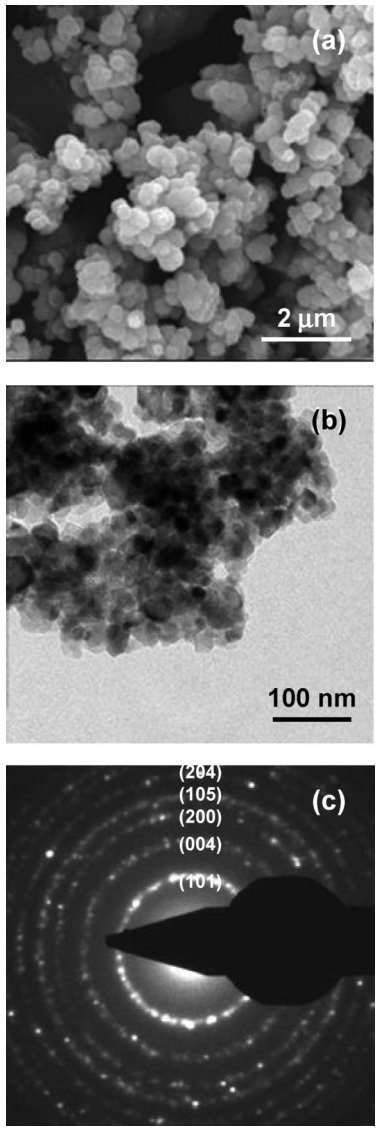

Figure 1. Typical SEM (a) and TEM (b) images of sol−gel derived nanocrystalline anatase TiO_2. The corresponding SAED pattern has been presented in (c).

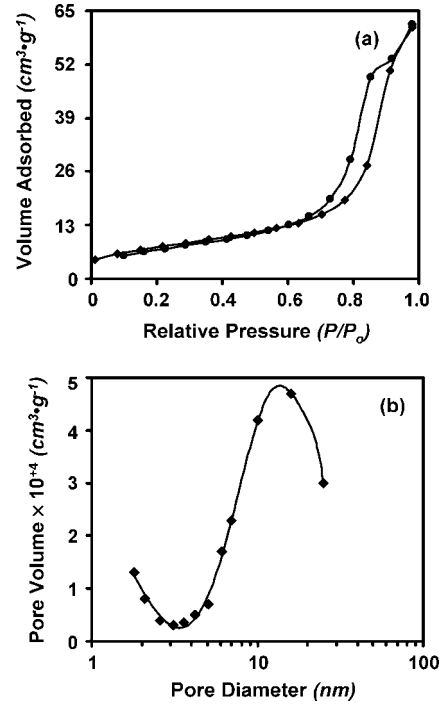

Figure 2. Typical N_2 adsorption/desorption isotherms (a) and BJH pore-size distribution curve (b) as obtained for the sol−gel derived nanocrystalline anatase TiO_2.

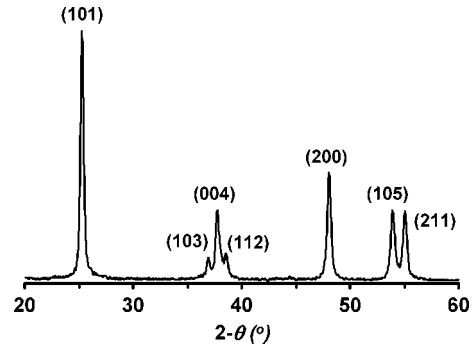

Figure 3. Typical broad-scan XRD pattern obtained for the sol−gel derived nanocrystalline anatase TiO_2.

are similar to that shown in Figure 3 and do not contain any additional peaks corresponding to Ag_2O and Ag^0.

Surface Chemistry of Pure and Ag_2O/Ag^0-Deposited Nanocrystalline Anatase TiO_2. The XPS broad-scan spectra obtained for Ag_2O/Ag^0-deposited nanocrystalline anatase TiO_2, processed via UV-reduction method, are presented in Figure 4 for different Ag-concentrations. In Figure 4, panels a and b, which corresponds to lower Ag concentrations, the presence of Ti, O, and C has been detected on the powder surface. (Note: The XPS broad-scan spectrum of pure nanocrystalline anatase TiO_2 is similar those shown in Figure 4, panels a and b; hence, it is not presented here). The broad-scan analyses could not reveal the presence of Ag on the powder surface although change in the color of pure anatase TiO_2 after the Ag deposition could be clearly observed for all Ag concentrations. However, the presence of Ag could be detected in Figure 4, panels c and d, which correspond to higher Ag concentrations. The intensity of Ag (3d) peak is noted to increase with increasing Ag concentration suggesting the deposition of relatively larger amount of Ag at higher Ag concentrations.

The narrow-scan analyses of Ag $3d_{5/2}$ obtained for Ag_2O/Ag^0-deposited nanocrystalline anatase TiO_2, processed via UV-reduction method, are presented in Figure 5 for different Ag concentrations. It is observed that, typically for lower Ag concentration (0.1 mol %), the presence of Ag could be detected on the powder surface via narrow-scan analysis, Figure 5a, which was not possible via broad-scan analysis, Figure 4. The deconvolution of Ag $3d_{5/2}$ peaks for all powders shows that, due to their asymmetric nature, the presence of two subpeaks could be revealed and the related BE levels have been tabulated in Table 1. The subpeaks at higher and lower BE levels are assigned to Ag^0 and Ag_2O species.[9,13,14] It is interesting to note that, the BE level of Ag^0 has been shifted by 0.3−0.5 eV relative to the bulk value of 368.2 eV.

The broad-scan XPS spectra, obtained for Ag_2O/Ag^0-deposited nanocrystalline anatase TiO_2, processed via chemical-reduction (using Sn^{2+} ions) method, are presented in Figure 6 for different Ag concentrations. Comparison of Figures 4 and 6 shows that, for the present Ag-deposition method, in addition to Ti, O, and C, the presence of Sn is also detected on the powder surface. Moreover, similar to the previous case, in Figure 6a−c which correspond to relatively lower Ag concentrations, the Ag (3d) peak could not be observed using the broad-scan analysis except for the highest Ag concentration, Figure 6d.

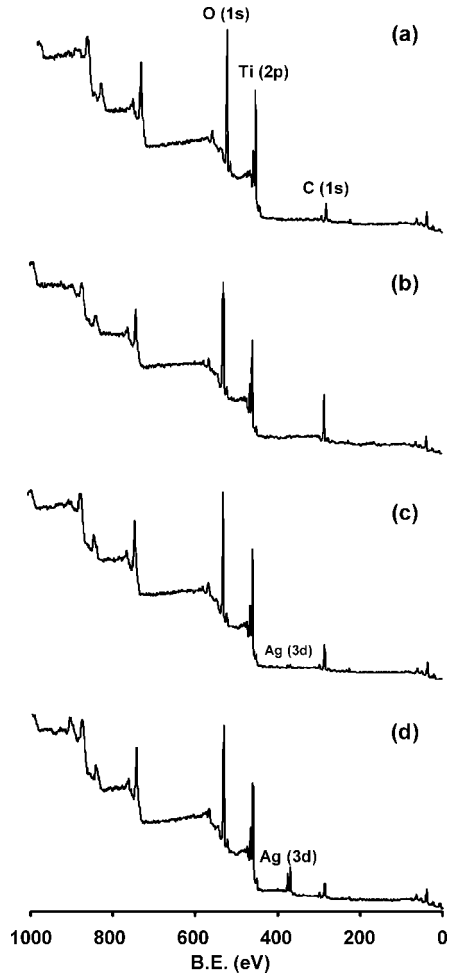

Figure 4. Broad-scan XPS spectra obtained for Ag_2O/Ag^0-deposited nanocrystalline anatase TiO_2 processed via UV-reduction method. The Ag concentration is varied as (a) 0.01, (b) 0.1, (c) 1.0, and (d) 10 mol %.

The narrow-scan Sn (3d) spectra obtained for Ag_2O/Ag^0-deposited nanocrystalline anatase TiO_2, processed via chemical-reduction (using Sn^{2+} ions) method, are presented in Figure 7 for different Ag concentrations. The deconvolution of symmetric Sn (3d) spectra reveals the presence of only one subpeak and the related BE positions of Sn $3d_{5/2}$ have been tabulated in Table 1. It is observed that the BE levels of Sn $3d_{5/2}$ increase with increasing Ag concentration, which are assigned to the presence of either Sn^{2+} ions or SnO_2 on the powder surface.[33]

The narrow-scan spectra of Ag $3d_{5/2}$, obtained for Ag_2O/Ag^0-deposited nanocrystalline anatase TiO_2 processed via chemical-reduction (using Sn^{2+} ions) method, are presented in Figure 8 for two different Ag concentrations. It is observed that similar to the previous case, the deconvolution of obtained spectra for lower Ag concentration, Figure 8a, reveals the presence of two subpeaks which are assigned to Ag^0 and AgO/Ag_2O species, Table 1.[9,13,14] However, for the highest Ag concentration, Figure 8b, due to the symmetric nature of the peak and its lower full-width at half-maximum (fwhm) intensity of 1.6, the deconvolution reveals the presence of only one subpeak, which is assigned to the presence of Ag_2O only. The narrow scan analyses, Figures 7 and 8, thus suggest the presence of SnO_2 and absence of Ag^0 on the surface of Ag_2O/Ag^0-deposited nanocrystalline anatase TiO_2 processed via chemical-reduction (using Sn^{2+} ions) method with the highest Ag concentration of 10 mol %.

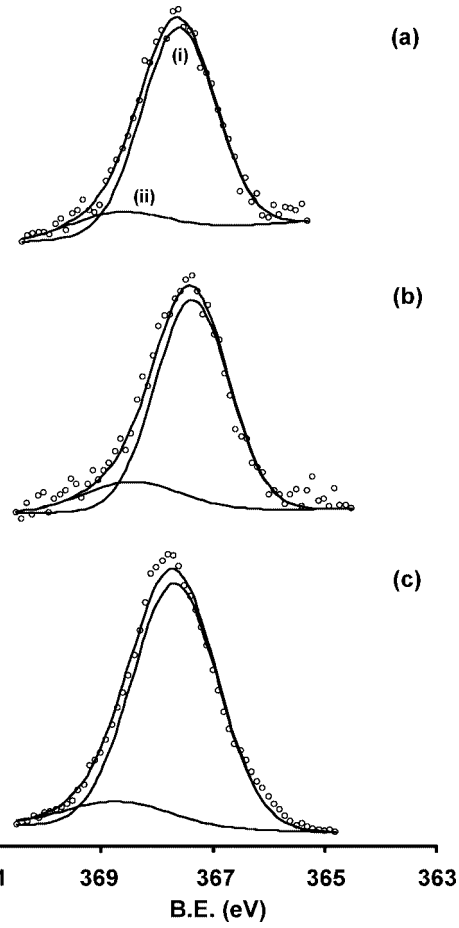

Figure 5. Narrow-scan Ag $3d_{5/2}$ XPS spectra obtained for Ag_2O/Ag^0-deposited nanocrystalline anatase TiO_2 processed via UV-reduction method. The Ag concentration is varied as (a) 0.1, (b) 1.0, and (c) 10 mol %. (i) Ag_2O and (ii) Ag^0.

TABLE 1: BE Levels of Sn $3d_{5/2}$ and Ag $3d_{5/2}$ as Obtained from the Surface of Ag_2O/Ag^0-Deposited Nanocrystalline Anatase TiO_2 Processed via Two Different Methods

deposition method	amount of Ag (mol %)	Sn $3d_{5/2}$ (eV)	Ag $3d_{5/2}$ (eV) lower-peak	Ag $3d_{5/2}$ (eV) upper-peak
UV reduction	0.01		not detectable	
	0.1		367.7 (Ag_2O)	368.7 (Ag^0)
	1.0		367.4 (Ag_2O)	368.5 (Ag^0)
	10		367.7 (Ag_2O)	368.7 (Ag^0)
chemical reduction (using Sn^{2+} ions)	0.01	486.4 (Sn^{2+})	not detectable	
	0.1	486.4 (Sn^{2+})	not detectable	
	1.0	486.6 (SnO_2)	367.2 (AgO)	368.3 (Ag^0)
	10	486.8 (SnO_2)	367.5 (Ag_2O)	

Photoabsorption Characteristics of Pure and Ag_2O/Ag^0-Deposited Nanocrystalline Anatase TiO_2. The DR absorption spectra of pure and Ag_2O/Ag^0-deposited nanocrystalline anatase TiO_2, obtained via two different techniques, are presented in Figure 9. The pure nanocrystalline anatase TiO_2 shows an enhanced photoabsorption in the UV region below 400 nm with the bang gap of 3.37 eV estimated using eq 2, which suggests an increase in the band gap relative to the bulk value of 3.2 eV. For Ag_2O/Ag^0-deposited nanocrystalline anatase TiO_2 obtained via UV-reduction method, with increasing Ag concentration, Figure 9a, the fundamental band gap is observed to remain the same; however, it shows an enhanced photoabsorption in the visible region (400−800 nm). This absorption peak in the visible region is observed to become more intense and

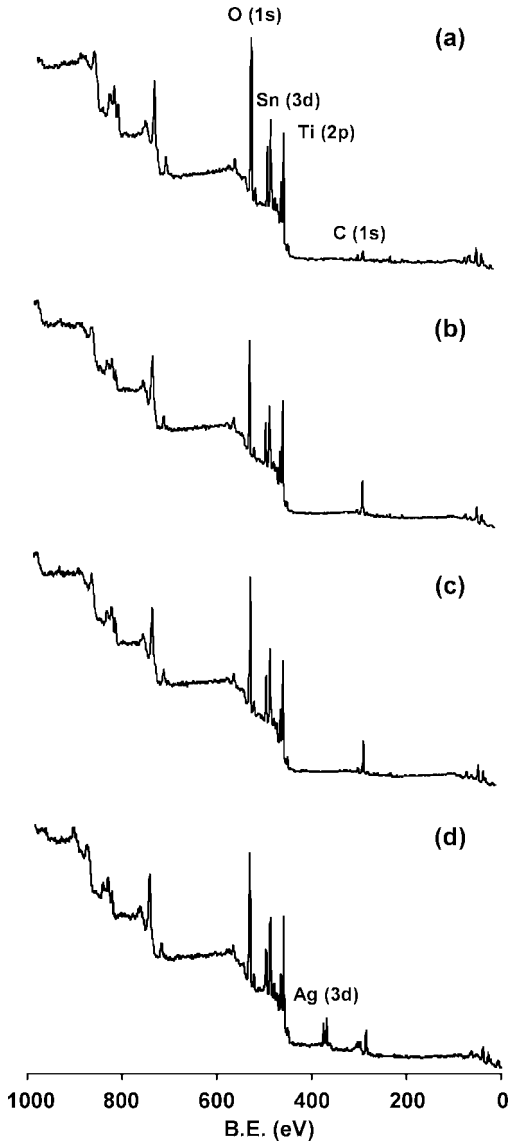

Figure 6. Broad-scan XPS spectra obtained for Ag_2O/Ag^0-deposited nanocrystalline anatase TiO_2 processed via chemical-reduction (using Sn^{2+} ions) method. The Ag concentration is varied as (a) 0.01, (b) 0.1, (c) 1.0, and (d) 10 mol %.

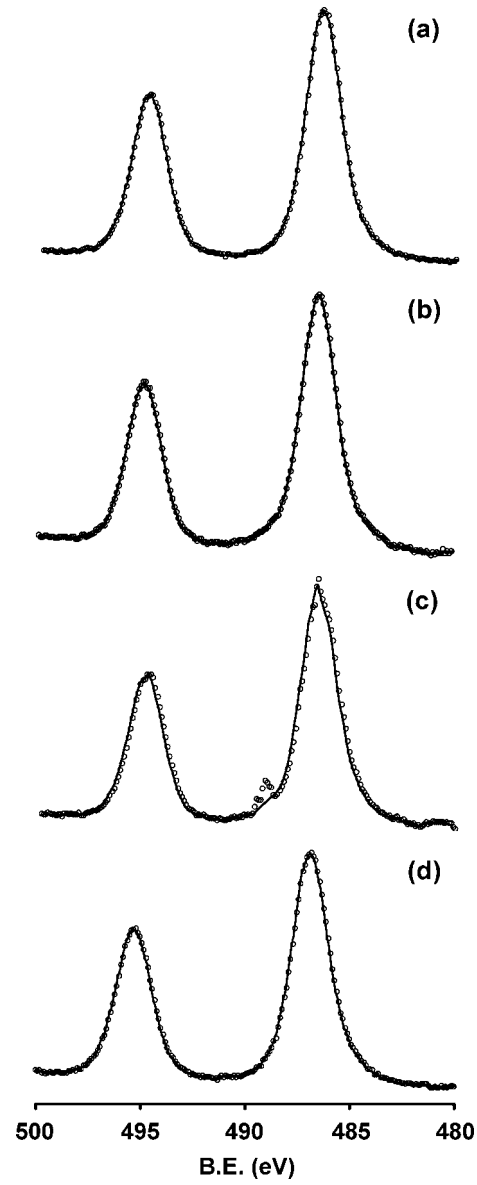

Figure 7. Narrow-scan Sn (3d) XPS spectra obtained for Ag_2O/Ag^0-deposited nanocrystalline anatase TiO_2 processed via chemical-reduction (using Sn^{2+} ions) method. The Ag concentration is varied as (a) 0.01, (b) 0.1, (c) 1.0, and (d) 10 mol %.

broader along with the progressive red shift with increasing Ag concentration within the investigated range.

For Ag_2O/Ag^0-deposited nanocrystalline anatase TiO_2, obtained via chemical-reduction (using Sn^{2+} ions) method, Figure 9b, the absorption peak in the visible region is observed only for the highest Ag concentration (10 mol %). Comparison of Figure 9, panels a and b, shows that, for the same Ag concentration of 10 mol %, the absorption peak in the visible region for the chemical-reduction (using Sn^{2+} ions) method is relatively less intense than that for the UV-reduction method.

Photoemission Characteristics of Pure and Ag_2O/Ag^0-Deposited Nanocrystalline Anatase TiO_2. The room temperature PL spectra of pure and Ag_2O/Ag^0-deposited nanocrystalline anatase TiO_2, obtained via two different techniques, are presented in Figure 10. For the pure nanocrystalline anatase TiO_2, a broad PL spectrum is observed which peaks at 433 nm. For Ag_2O/Ag^0-deposited nanocrystalline anatase TiO_2 processed via UV-reduction method, Figure 10a, with increasing Ag concentration the PL intensity is seen to be progressively quenched, with a red shift to 496 nm for two lower Ag concentrations (0.01 and 0.1 mol %). Progressive quenching of PL intensity is also noted for Ag_2O/Ag^0-deposited nanocrystalline anatase TiO_2 processed via chemical-reduction (using Sn^{2+} ions) method, Figure 10b, except that the PL intensity is initially enhanced for the lowest Ag concentration of 0.01 mol % relative to that of pure nanocrystalline anatase TiO_2.

In Figure 11, the PL intensity of surface-sensitized nanocrystalline anatase TiO_2 is compared with that of pure and Ag_2O/Ag^0-deposited nanocrystalline anatase TiO_2 processed via chemical-reduction (using Sn^{2+}-ions) method having the lowest Ag-concentration of 0.01 mol %. It is noted that, the PL intensity of surface-sensitized nanocrystalline anatase TiO_2 is much higher relative to that of pure nanocrystalline anatase TiO_2. The surface-deposition of Ag_2O/Ag^0 reduces the PL intensity; however, it remains slightly higher than that of pure nanocrystalline anatase TiO_2.

Photocatalytic Activity of Pure and Ag_2O/Ag^0-Deposited Nanocrystalline Anatase TiO_2. ***MB Adsorption in the Dark.*** The variation in amount of MB adsorbed on the surface of pure and Ag_2O/Ag^0-deposited nanocrystalline anatase TiO_2, processed

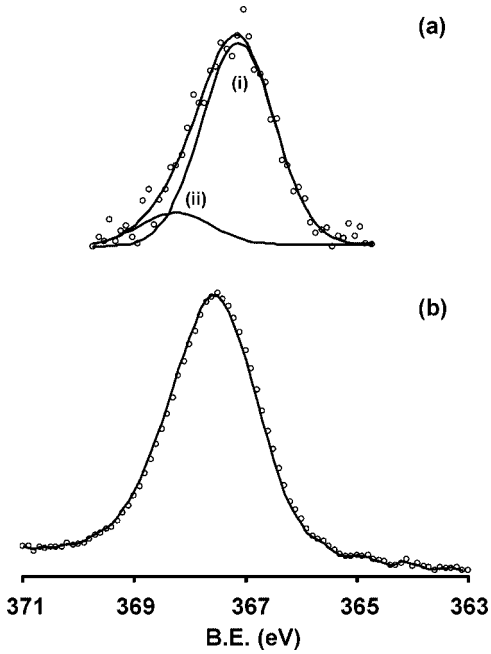

Figure 8. Narrow-scan Ag $3d_{5/2}$ XPS spectra obtained for Ag_2O/Ag^0-deposited nanocrystalline anatase TiO_2 processed via chemical-reduction (using Sn^{2+} ions) method. The Ag concentration is varied as (a) 1.0 and (b) 10 mol %. (i) Ag_2O and (ii) Ag^0.

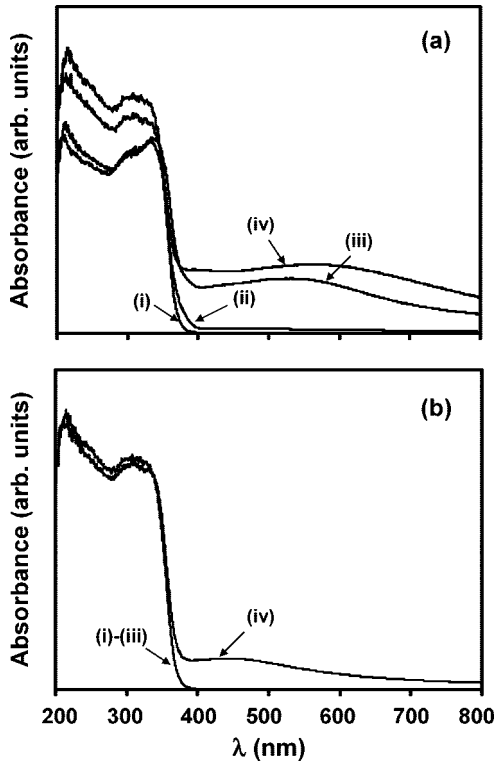

Figure 9. DR absorbance spectra obtained for Ag_2O/Ag^0-deposited nanocrystalline anatase TiO_2 processed via UV reduction (a) and chemical-reduction (using Sn^{2+} ions) (b) methods. The Ag concentration is varied as (i) 0.01, (ii) 0.1, (iii) 1.0, and (iv) 10 mol %. The spectrum for pure nanocrystalline anatase TiO_2 is similar to that of (i).

via two different techniques, is presented in Figure 12. As indicated by the dotted line, 19.2% MB is adsorbed on the surface of pure nanocrystalline anatase TiO_2 after stirring in the dark before the UV-radiation exposure. The Ag deposition with the lowest concentration of 0.01 mol % decreases the amount of surface-adsorbed MB for both the deposition

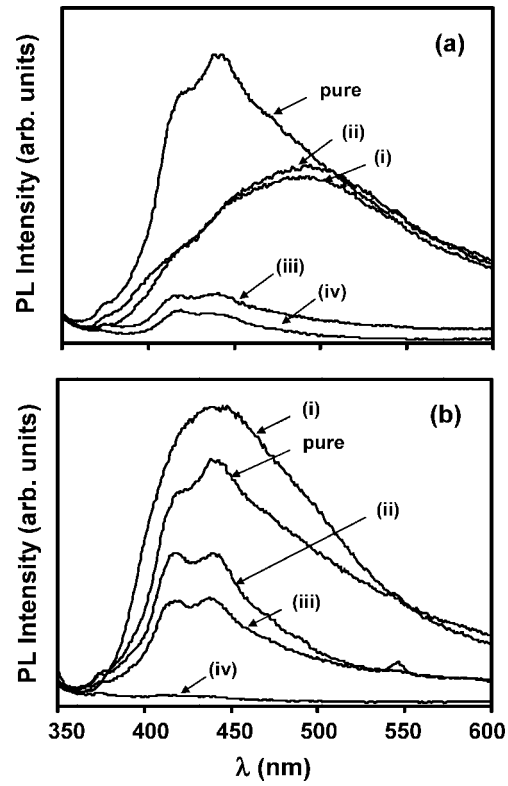

Figure 10. PL spectra obtained for pure and Ag_2O/Ag^0-deposited nanocrystalline anatase TiO_2 processed via UV-reduction (a) and chemical-reduction (using Sn^{2+} ions) (b) methods. The Ag concentration is varied as (i) 0.01, (ii) 0.1, (iii) 1.0, and (iv) 10 mol %.

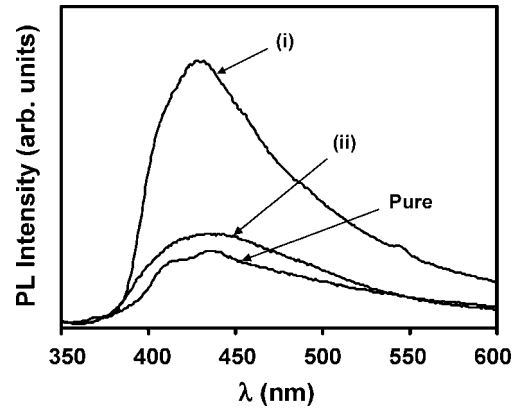

Figure 11. PL spectra obtained for the pure, surface-sensitized (i), and Ag_2O/Ag^0-deposited nanocrystalline anatase TiO_2 processed via chemical-reduction (using Sn^{2+}-ions) method with the lowest Ag concentration of 0.01 mol % (ii).

methods. The decrease is observed to be larger for the UV-reduction method than that for the chemical-reduction (using Sn^{2+} ions) method. With increasing Ag concentration, the amount of surface-adsorbed MB increases for both the deposition techniques. For the highest Ag concentration of 10 mol %, however, a sudden decrease in the amount of surface-adsorbed MB is noted for the chemical-reduction (using Sn^{2+} ions) method. As a result, within the investigated range of Ag concentration, the maximum amount of surface adsorption of MB is observed for 10 and 1 mol % Ag for the UV-reduction and chemical-reduction (using Sn^{2+} ions) methods.

Determination of Apparent First-Order Reaction Rate Constant (k_{app}). The variation in residual MB concentration as a function of UV-radiation exposure time for the pure and $Ag_2O/$

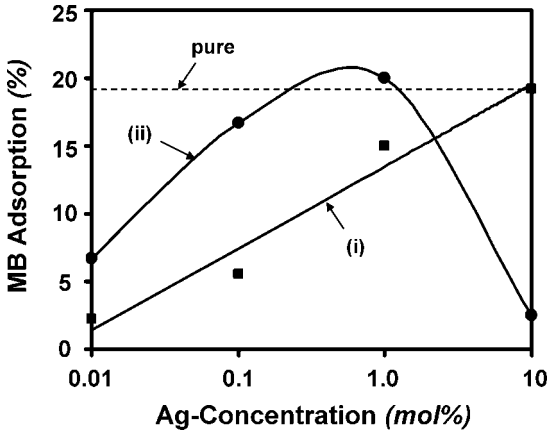

Figure 12. Variation in the amount of surface-adsorbed MB as a function of Ag concentration for Ag_2O/Ag^0-deposited nanocrystalline anatase TiO_2, processed via UV-reduction (i) and chemical-reduction (using Sn^{2+} ions) (ii) methods. The dotted line indicates the amount of MB adsorbed by pure nanocrystalline anatase TiO_2.

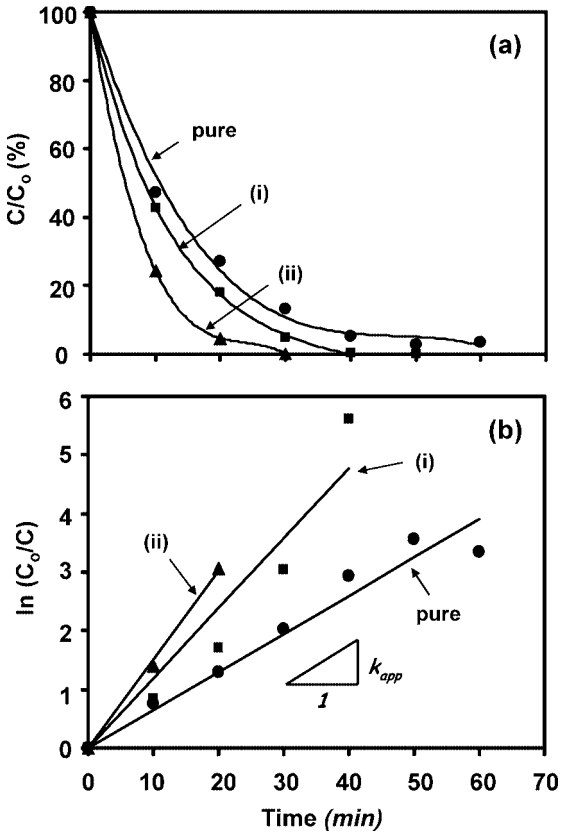

Figure 13. (a) Variation in the residual MB concentration as a function of UV-radiation exposure time for pure and Ag_2O/Ag^0-deposited nanocrystalline anatase TiO_2, processed via UV-reduction method. The Ag concentration is varied as (i) 0.1 and (ii) 10 mol %. (b) Corresponding plots for determining k_{app}.

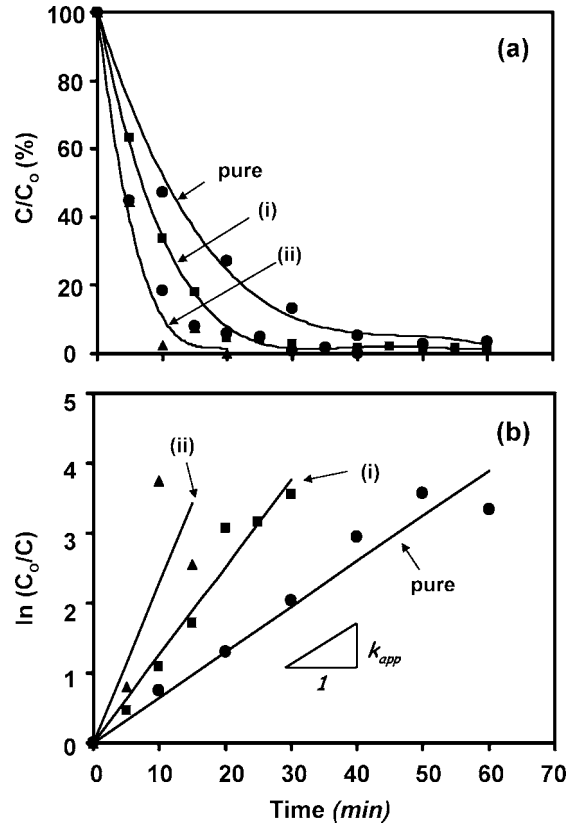

Figure 14. (a) Variation in the residual MB concentration as a function of UV-radiation exposure time for pure and Ag_2O/Ag^0-deposited nanocrystalline anatase TiO_2 processed via chemical-reduction (using Sn^{2+} ions) method. The Ag concentration is varied as (i) 0.01 and (ii) 0.1 mol %. (b) Corresponding plots for determining k_{app}.

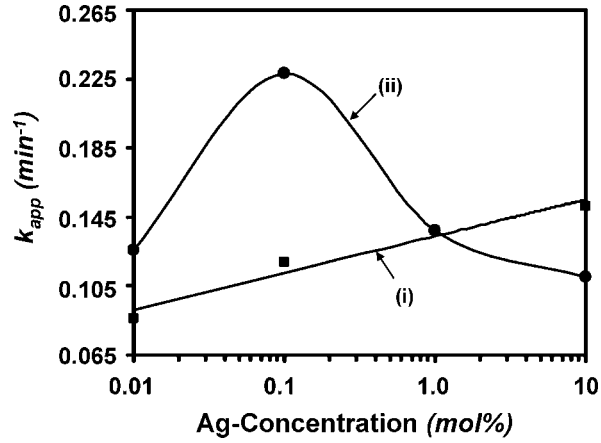

Figure 15. Variation in k_{app} as a function of Ag-concentration for Ag_2O/Ag^0-deposited nanocrystalline anatase TiO_2 processed via UV-reduction (i) and chemical-reduction (using Sn^{2+} ions) (ii) methods. k_{app} value for pure nanocrystalline anatase TiO_2 is 0.065 min^{-1}.

Ag^0-deposited nanocrystalline anatase TiO_2, processed via UV-reduction and chemical-reduction (using Sn^{2+} ions) methods, is presented in Figures 13a and 14a. The corresponding plots for determining k_{app} are presented in Figures 13b and 14b. It is noted that Ag_2O/Ag^0-deposited nanocrystalline anatase TiO_2, processed under different conditions, is highly photocatalytically active as evidenced by the degradation of MB with increasing UV-radiation exposure time. Moreover, all surface-modified powders are photocatalytically more active than pure nanocrystalline anatase TiO_2. The k_{app} values are estimated from the slopes of curve-fitted straight lines presented in Figures 13b and 14b.

The variation in k_{app} as a function of Ag concentration, obtained for the pure and Ag_2O/Ag^0-deposited nanocrystalline anatase TiO_2 processed via two different techniques, is presented in Figure 15. The k_{app} value for the pure nanocrystalline anatase TiO_2 is estimated to be 0.065 min^{-1} and those estimated for Ag_2O/Ag^0-deposited nanocrystalline anatase TiO_2 processed via UV-reduction and chemical-reduction (using Sn^{2+} ions) methods lie within the range of 0.086−0.151 and 0.11−0.228 min^{-1},

which are higher than that of pure nanocrystalline anatase TiO_2. Moreover, k_{app} values are higher for Ag_2O/Ag^0-deposited nanocrystalline anatase TiO_2 processed via chemical-reduction (using Sn^{2+} ions) method than those processed via UV-reduction method except for the highest Ag concentration of 10 mol %.

It is further noted that k_{app} increases initially with increasing Ag-concentration for both the deposition methods. However, for Ag_2O/Ag^0-deposited nanocrystalline anatase TiO_2 processed via chemical-reduction (using Sn^{2+} ions) method, k_{app} reaches the maximum value of 0.228 min^{-1} at 0.1 mol % Ag and then decreases with further increase in Ag concentration. On the other hand, for Ag_2O/Ag^0-deposited nanocrystalline anatase TiO_2 processed via UV-reduction method, k_{app} increases continuously and reaches the maximum value of 0.151 min^{-1} at 10 mol % Ag. Interestingly, the nature of variation in k_{app}, Figure 15, is almost similar to that in the amount of surface-adsorbed MB, Figure 12, as a function of Ag concentration.

Discussion

Synthesis of Sol−Gel Derived Pure Nanocrystalline Anatase TiO_2. In the present investigation, the nanocrystalline anatase TiO_2 has been synthesized via sol−gel using the *R* value of 90, which is the ratio of molar concentration of water to that of alkoxide precursor, as this value of *R* has been demonstrated earlier to give the maximum photocatalytic activity.[30,31] The hydrolysis and condensation reactions, which are responsible for the formation of nanocrystalline anatase TiO_2 via sol−gel can be summarized as[29]

$$Ti(OC_3H_7)_4 + 4H_2O \rightarrow Ti(OH)_4 + 4C_3H_7OH \quad (5)$$

$$Ti(OH)_4 \rightarrow TiO_2 + 2H_2O \quad (6)$$

The net reaction is,

$$Ti(OC_3H_7)_4 + 2H_2O \rightarrow TiO_2 + 4C_3H_7OH \quad (7)$$

The as-synthesized dried TiO_2 powder is amorphous and gets crystallized completely into anatase TiO_2 following the calcination at 600 °C as revealed using the SAED and XRD analyses. The stabilization of metastable anatase phase at room temperature in the undoped nanocrystalline TiO_2 can be explained based on the size dependent anatase-to-rutile phase transformation,[29] which is supported here using TEM analysis. The small nanocrystallite size of anatase TiO_2 has also been reflected in wider band gap which is +0.17 eV larger than the bulk value, consistent with the experimentally observed band gap enhancement below a critical size of ∼17 nm as reported in the literature.[34,35]

The pure nanocrystalline anatase TiO_2 shows photoabsorption only in the UV range below 400 nm. Moreover, PL from the sol−gel derived nanocrystalline anatase TiO_2 is a broad spectrum in the visible region peaking at ∼433 nm, which suggests the presence of large concentration of oxygen-ion vacancies, which mediate the recombination of photoinduced e^-/h^+ pairs.[36,37] The excess oxygen-ion vacancies are known to be created at room temperature within the nanocrystallites of semiconductor oxides below a critical size.[38] Higher concentration of oxygen-ion vacancies (V_0), produced as a result of size-effect, is in turn responsible for the formation of excess surface-concentration of superoxide ions (O_2^-, O^-) following oxygen-spillover reactions, in which the conduction band electrons are picked-up by oxygen from the surrounding atmosphere.[39]

$$O_2\,(gas) + V_0 + e^- \xrightarrow{Ag,\ TiO_2} O_2^-\,(ads) \quad (8)$$

$$\frac{1}{2}O_2\,(gas) + V_0 + e^- \xrightarrow{Ag,\ TiO_2} O^-\,(ads) \quad (9)$$

At room temperature, eq 8 is more favorable than the other reaction. In the case of Ag_2O/Ag^0-deposited nanocrystalline anatase TiO_2, the spillover of oxygen via eqs 8 and 9 is catalyzed by the presence of Ag^0.[14,40] The formation of superoxide ions results in negatively charged surface with the positively charged metal-cations located just below it thus creating a space-charge layer, which plays a major role in the surface adsorption of MB, and hence, the photocatalytic activity of nanocrystalline anatase TiO_2.

Comparison of Two Different Mechanisms Used for Processing Ag_2O/Ag^0-Deposited Nanocrystalline Anatase TiO_2. To enhance the photocatalytic activity, Ag_2O/Ag^0 have been deposited with different Ag concentrations on the surface of sol−gel derived nanocrystalline anatase TiO_2 using the UV-reduction and chemical-reduction (using Sn^{2+} ions) techniques.

UV-Reduction Method. In this method, the addition of ammonium hydroxide to an aqueous $AgNO_3$ solution results in the formation of silver ammonia complex ions via following reactions[28,41]

$$NH_4OH\,(aq) \rightarrow NH_3\,(aq) + H_2O \quad (10)$$

$$Ag^+\,(aq) + 2NH_3\,(aq) \xrightarrow{TiO_2} [Ag(NH_3)_2]^+\,(ads) \quad (11)$$

The net reaction can be written as

$$Ag^+\,(aq) + 2NH_4OH\,(aq) \xrightarrow{TiO_2} [Ag(NH_3)_2]^+\,(ads) + 2H_2O \quad (12)$$

The addition of nanocrystalline anatase TiO_2 to the above solution results in the surface adsorption of silver ammonia complex ions due to the presence of space-charge layer. When the suspension is illuminated with UV radiation, e^-/h^+ pairs are effectively created within the nanocrystalline anatase TiO_2. The photoinduced electrons then reduce the surface-adsorbed silver ammonia complex ions to metallic Ag^0.

$$[Ag(NH_3)_2]^+\,(ads) + e^- \xrightarrow{TiO_2,\ UV} Ag^0 + 2NH_3\,(aq) \quad (13)$$

The overall reaction for the Ag^0 deposition on the surface of nanocrystalline anatase TiO_2 via UV-reduction method can be written as

$$Ag^{+} + 2NH_4OH + e^{-} \xrightarrow{TiO_2,\ UV} Ag^{0} + 2NH_3 + 2H_2O \quad (14)$$

The shift in Ag $3d_{5/2}$ BE level by $+0.3-0.5$ eV relative to the bulk value, as revealed by the XPS analysis (Table 1), suggests the presence of Ag^0 nanoparticles with size less than 10 nm, which may exhibit the positive core-level BE shift as a result of "cluster-size" effect involving the initial and final state effects during the XPS analysis.[42] In the presence of space charge layer on the surface of nanocrystalline anatase TiO_2, the deposited Ag^0 however gets oxidized immediately to Ag_2O (or AgO) via "reverse-spillover" effect.[13,43]

$$4Ag^{0} + O_2^{-}\,(ads) \xrightarrow{TiO_2} 2Ag_2O + e^{-} \quad (15)$$

$$2Ag^{0} + O^{-}\,(ads) \xrightarrow{TiO_2} Ag_2O + e^{-} \quad (16)$$

The deposition of Ag_2O/Ag^0 on the surface of nanocrystalline anatase TiO_2 via UV-reduction method has been confirmed here using the XPS analysis (Figure 5), where the amount of Ag_2O is found to be relatively larger than that of Ag^0. Hence, in the present investigation, the reverse-spillover effect appears to be a dominant oxidation mechanism of deposited Ag^0.

Chemical-Reduction (Using Sn^{2+} Ions) Method. The difference between this deposition technique and the previous one is the nature of reducing agent used. In the previous case, the photoinduced electrons within the nanocrystalline anatase TiO_2 are the reducing agent, whereas in the present case, the surface-adsorbed Sn^{2+} ions are the reducing agent.

When the pure nanocrystalline anatase TiO_2 is added to an aqueous solution of $SnCl_2$, it adsorbs Sn^{2+} ions on the surface (surface-sensitization) due to the presence of space charge layer. When the surface-sensitized nanocrystalline anatase TiO_2 is stirred in an aqueous solution containing the silver-ammonia complex ions, it results in the deposition of metallic Ag^0 on the surface via the following chemical reaction:

$$2[Ag(NH_3)_2]^{+}\,(ads) + Sn^{2+}\,(ads) \xrightarrow{TiO_2} 2Ag^{0} + 4NH_3\,(aq) + Sn^{4+}\,(ads) \quad (17)$$

Larger amount of deposited-Ag^0 gets oxidized by the superoxide ions via reverse-spillover effect, eqs 15 and 16, as indicated by the XPS analysis (Figure 8). The XPS data (Table 1) also suggests that for larger Ag-concentrations (1 and 10 mol %) relatively more amount of Sn^{4+} ions, generated during the reduction process (eq 17), get converted to SnO_2 via reverse-spillover effect

$$Sn^{4+} + 4O_2^{-}\,(ads) \xrightarrow{TiO_2} SnO_2 + 3O_2\,(gas) \quad (18)$$

$$Sn^{4+} + 4O^{-}\,(ads) \xrightarrow{TiO_2} SnO_2 + O_2\,(gas) \quad (19)$$

The formation of Ag_2O and SnO_2, at higher Ag concentrations, may drastically reduce the surface-concentration of superoxide ions, which is reflected here in the reduced amount of surface-adsorbed MB under these conditions, as discussed in detail later.

Comparison of Photoabsorption and Photoemission Characteristics. ***UV-Reduction Method.*** The DR absorption spectra obtained for Ag_2O/Ag^0-deposited nanocrystalline anatase TiO_2, processed via UV-reduction method, show a gradual increase in absorption in the visible-region (400−800 nm) with increasing Ag-concentration (Figure 9a). This is in contrast to the pure nanocrystalline anatase TiO_2, which shows absorption only in the UV region below 400 nm. In the literature, absorption in the visible region for Ag_2O/Ag^0-deposited nanocrystalline TiO_2 has been attributed to the surface plasmon absorption due to the spatially confined electrons in the deposited-Ag^0 nanoparticles.[9,13,14,44] Since the band gap of Ag_2O is 1.3−1.5 eV, absorption in the visible region may also be contributed by Ag_2O. Moreover, in the literature, more intense, broader, and red-shifted absorbance peaks in the visible region have been ascribed to relatively larger average size and broader size distribution of Ag^0 nanoparticles, high refractive index of TiO_2, and interaction between Ag^0 and TiO_2.[44] Hence, from the absorption spectra obtained for Ag_2O/Ag^0-deposited nanocrystalline anatase TiO_2 processed via UV-reduction method, it is inferred that the average nanoparticle size, size distribution, and surface coverage by Ag_2O/Ag^0 increases with increasing Ag concentration.

It is also noted that PL from Ag_2O/Ag^0-deposited nanocrystalline anatase TiO_2, processed via UV-reduction method (Figure 10a), is progressively quenched with increasing Ag concentration relative to that of pure nanocrystalline anatase TiO_2. Such PL quenching has been attributed to an enhanced photoinduced e^-/h^+ lifetime caused by the effective trapping of photoinduced electrons by the deposited Ag_2O/Ag^0.[14,36,37] This suggests an increasing photoinduced e^-/h^+ lifetime with increasing Ag concentration, which is conducive in enhancing the photocatalytic activity of Ag_2O/Ag^0-deposited nanocrystalline anatase TiO_2, processed via UV-reduction method, relative to that of pure nanocrystalline anatase TiO_2.

Chemical-Reduction (using Sn^{2+} Ions) Method. The DR absorption spectra obtained for Ag_2O/Ag^0-deposited nanocrystalline anatase TiO_2, processed via chemical-reduction (using Sn^{2+} ions) method (Figure 9b), show absorption in the visible region only for the highest Ag-concentration of 10 mol %. Comparison of photoabsorption spectra for the two Ag-deposition methods, corresponding to the same Ag concentration of 10 mol % suggests that, the average nanoparticle size, size distribution, and surface coverage of Ag_2O/Ag^0 are relatively lesser for the chemical-reduction (using Sn^{2+} ions) method compared to those with the UV-reduction method.

Similar to the previous case (except for the lowest Ag-concentration of 0.01 mol %), with increasing Ag concentration, PL from Ag_2O/Ag^0-deposited nanocrystalline anatase TiO_2, processed via chemical-reduction (using Sn^{2+} ions) method (Figure 10b), is progressively quenched relative to that of pure nanocrystalline anatase TiO_2. However, relative to the PL intensity of the surface-sensitized sample (Figure 11), progressive reduction in the PL intensity is noted within the entire range of Ag concentration investigated here. This again suggests an enhanced photoinduced e^-/h^+ lifetime with increasing Ag

concentration for Ag_2O/Ag^0-deposited nanocrystalline anatase TiO_2 processed via chemical-reduction (using Sn^{2+} ions) method.

The surface chemistry, as revealed by XPS analysis (Figure 6), suggests the additional presence of Sn^{2+} ions on the surface of Ag_2O/Ag^0-deposited nanocrystalline anatase TiO_2 processed via chemical-reduction (using Sn^{2+} ions) method. Moreover, the surface-sensitized nanocrystalline anatase TiO_2 shows very high PL intensity than that of pure nanocrystalline anatase TiO_2 (Figure 11). This strongly suggests that, for the surface-sensitized sample, as a result of charge balance due to the surface adsorption of Sn^{2+}-ions, an excess surface concentration of oxygen-ion vacancies has been possibly generated, which mediate the photoinduced e^-/h^+ recombination process, thus enhancing the PL intensity. However, following Ag_2O/Ag^0 deposition with the lowest Ag concentration of 0.01 mol %, the PL intensity decreases relative to that of surface-sensitized nanocrystalline anatase TiO_2. This has been possibly contributed by two factors. First, Ag_2O/Ag^0 deposition converts some of Sn^{2+} into Sn^{4+} ions, eq 17, which possibly reduces the excess surface concentration of oxygen-ion vacancies, which in turn reduces the PL intensity. Second, the deposited Ag_2O/Ag^0 provide effective sites for trapping the photoinduced electrons; thus, increasing the photoinduced e^-/h^+ lifetime, which may also reduce the PL intensity. However, the PL intensity for the lowest Ag-concentration of 0.01 mol % still remains higher than that for pure nanocrystalline anatase TiO_2 (Figure 11), which may be attributed to the balance between the opposite effects of dependence of photoinduced e^-/h^+ lifetime on the concentration of Sn^{2+} ions and amount of Ag_2O/Ag^0 present on the powder surface.

Comparison of Surface Adsorption of MB. As discussed earlier, the formation of negatively charged superoxide ions on the surface of pure nanocrystalline anatase TiO_2 results in the creation of space-charge layer. This space-charge layer is responsible for the surface-adsorption of MB dye molecules, which are cationic in an aqueous solution.[45,46] Hence, it is obvious that variation in the surface concentration of superoxide ions would affect the surface-adsorption of MB and, hence, the photocatalytic activity of nanocrystalline anatase TiO_2.

UV-Reduction Method. As shown by the dotted line in Figure 12, the sol−gel derived pure nanocrystalline anatase TiO_2 adsorbs 19.2% MB on the surface before exposure to UV radiation. When Ag_2O/Ag^0 are surface deposited via UV-reduction method, with the lowest Ag concentration of 0.01%, a drastic reduction in the amount of surface-adsorbed MB is noted as the concentration of potential surface-adsorption sites for MB, namely the superoxide ions, is possibly significantly reduced due to the formation of significant amount of Ag_2O via reverse-spillover effect, eqs 15 and 16.

The MB adsorption is however noted to increase, almost linearly, with increasing Ag concentration within the range of 0.01−10 mol %. It is well known that Ag^0 acts as a catalyst for the spillover of oxygen on the surface of nanocrystalline anatase TiO_2, eqs 8 and 9.[14,40] Larger the surface coverage of Ag^0 catalyst, stronger would be the oxygen-spillover effect. It appears that, with increasing Ag concentration, the loss in the concentration of superoxide ions due to the formation of a significant amount of Ag_2O is gradually compensated by an enhanced oxygen-spillover effect of Ag^0 and the superoxide formation on the surface of Ag_2O.[14] As a result, the amount of MB adsorbed on the powder surface increases with increasing Ag concentration within the investigated range of 0.01−10 mol %, which is highly favorable in enhancing the photocatalytic activity.

Chemical-Reduction (using Sn^{2+} Ions) Method. In this case as well, similar to the previous method, for the lowest Ag concentration of 0.01 mol %, decrease in the amount of surface-adsorbed MB is noted due to Ag_2O/Ag^0 deposition, which consumes the potential sites for the MB adsorption. However, the amount of MB adsorbed is relatively larger than that observed in the previous case. According to eqs 8 and 9, an excess surface concentration of oxygen-ion vacancies, produced as a result of the charge balance due to the presence of Sn^{2+} ions, possibly leads to higher surface concentration of superoxide ions, which in turn increases the amount of surface-adsorbed MB. Within the Ag concentration range of 0.01−1 mol %, higher amount of surface-adsorbed MB for the present method relative to that for UV-reduction method (Figure 12) is hence attributed to higher surface concentration of superoxide ions caused by the presence of Sn^{2+} ions. This effect of Sn^{2+} ions is, however, absent for the UV-reduction method as Sn^{2+} ions are not involved in this reduction process.

For the highest Ag concentration of 10 mol %, sudden decrease in the amount of surface-adsorbed MB is noted, which is also not observed for the UV-reduction method. There are three possible major contributing factors to this effect. First, at the highest Ag concentration of 10 mol %, most of the Sn^{2+} ions present on the surface may have been utilized for reducing the silver ammonium complex ions to Ag_2O/Ag^0. As a result, an excess surface concentration of oxygen-ion vacancies, which was generated due the presence of Sn^{2+} ions, is eliminated which in turn reduced the surface concentration of superoxide ions. Second, the formation of SnO_2 has been detected for the highest Ag concentration (Table 1), which may also reduce the surface concentration of superoxide ions via reverse-spillover effect. Third, at the highest Ag concentration, the XPS spectrum (Figure 8b) shows the absence of Ag^0 on the powder surface for the chemical-reduction (using Sn^{2+} ions) method. This may relatively reduce the oxygen-spillover effect, thus reducing the surface concentration of superoxide ions.

The net effect of these three possible contributing factors is a drastic reduction in the surface concentration of superoxide ions, and hence, in the amount of surface-adsorbed MB, for the highest Ag concentration of 10 mol % for Ag_2O/Ag^0-deposited nanocrystalline anatase TiO_2 processed via chemical-reduction (using Sn^{2+} ions) method. This has a strong effect on variation in the photocatalytic activity as a function of Ag concentration for the Ag_2O/Ag^0-deposited nanocrystalline anatase TiO_2 processed via chemical-reduction (using Sn^{2+} ions) method, as discussed below.

Comparison of Photocatalytic Activity. In the absence of any surface catalyst, the photocatalytic activity of pure nanocrystalline anatase TiO_2 is highly dependent on the band gap variation in the connected nanocrystallites as a function of size distribution and phases involved.[31] In the present investigation, the pure nanocrystalline anatase TiO_2 exhibits a k_{app} value of 0.065 min^{-1}, which has been contributed by smaller nanocrystallite size having the distribution within the range of ∼15−30 nm, the mesoporous structure having an average pore size of ∼15 nm and relatively higher surface adsorption of MB (19.2%). In order to enhance the photocatalytic activity, Ag_2O/Ag^0 have been deposited on the surface of nanocrystalline anatase TiO_2 with varying Ag-concentrations via two different techniques.

UV-Reduction Method. Within the investigated Ag concentration range of 0.01−10 mol %, the photocatalytic activity of

Ag_2O/Ag^0-deposited nanocrystalline anatase TiO_2, processed via UV-reduction method, is higher than that of pure nanocrystalline anatase TiO_2 (Figure 15). Since the amount of MB adsorbed on the powder surface (2.2−19.2%) is lower than that adsorbed on the surface of pure nanocrystalline anatase TiO_2 (19.2%), the increased photocatalytic activity has been attributed to an enhanced photoinduced e^-/h^+ lifetime (Figure 10a) due to the effective trapping of photoinduced electrons by the deposited Ag_2O/Ag^0. Moreover, the photocatalytic activity increases almost linearly with increasing Ag concentration, which has been ascribed to the corresponding variation in the amount of surface-adsorbed MB as a function of Ag concentration (Figure 12).

Chemical-Reduction (using Sn^{2+} Ions) Method. Similar to the previous case, within the investigated Ag concentration range, the photocatalytic activity of Ag_2O/Ag^0-deposited nanocrystalline anatase TiO_2, processed via chemical-reduction (using Sn^{2+} ions) method, is higher than that of pure nanocrystalline anatase TiO_2. Since the amount of MB adsorbed on the powder surface (2.5−20%) is lower than that adsorbed on the surface of pure nanocrystalline anatase TiO_2 (19.2%), this has been again attributed to an enhanced photoinduced e^-/h^+ lifetime (Figure 10b) due to the effective trapping of photoinduced electrons by the deposited Ag_2O/Ag^0. Moreover, higher photocatalytic activity as observed for the chemical-reduction (using Sn^{2+} ions) method, relative to that observed for the UV-reduction method, has been attributed to an enhanced MB adsorption on the powder surface (Figure 12) for the present method. The photocatalytic activity is seen to increase first with increasing Ag-concentration and then to decrease at higher Ag concentrations (Figure 15). This trend in variation of the photocatalytic activity appears to be similar to that observed for the amount of surface-adsorbed MB (Figure 12). Hence, for the chemical-reduction (using Sn^{2+} ions) method as well, nature of the variation in the photocatalytic activity is governed primarily by the corresponding variation in the amount of surface-adsorbed MB as a function of Ag concentration.

Overall, it appears that for both of the reduction techniques investigated here, an enhanced photocatalytic activity of Ag_2O/Ag^0-deposited nanocrystalline anatase TiO_2, relative to that of pure nanocrystalline anatase TiO_2 is a result of an increased photoinduced e^-/h^+ lifetime caused by the effective trapping of photoinduced electrons by the deposited Ag_2O/Ag^0. On the other hand, variation in the photocatalytic activity as a function of Ag concentration is governed by the corresponding variation in the amount of surface-adsorbed MB as a function of Ag concentration.

Lastly, the maximum photocatalytic activity has been observed for 0.1 and 10 mol % Ag for the chemical-reduction (using Sn^{2+}-ions) and UV-reduction methods with the corresponding k_{app} values of 0.228 and 0.151 min^{-1}, which are 3.5 and 2.3 times larger than that of pure nanocrystalline anatase TiO_2. Hence, within the investigated Ag-concentration range, the chemical-reduction (using Sn^{2+} ions) method appears to be more effective than the UV-reduction method, for depositing Ag_2O/Ag^0 on the surface of sol−gel derived nanocrystalline anatase TiO_2 to enhance its photocatalytic activity under UV-radiation exposure.

Conclusions

Nanocrystalline anatase TiO_2 has been successfully synthesized via sol−gel using the R value of 90 and observed to be photocatalytically active ($k_{app} = 0.065$ min^{-1}) for the degradation of MB dye in an aqueous solution under UV-radiation exposure.

To enhance the photocatalytic activity, Ag_2O/Ag^0 have been deposited on the surface of nanocrystalline anatase TiO_2, with varying Ag concentration within the range of 0.01−10 mol % via two different techniques, namely the UV reduction and chemical reduction (using Sn^{2+} ions).

Within the investigated Ag-concentration range, Ag_2O/Ag^0-deposited nanocrystalline anatase TiO_2, processed via both techniques, exhibits higher photocatalytic activity than that of pure nanocrystalline anatase TiO_2 due to an enhanced photoinduced e^-/h^+ lifetime as a result of effective trapping of photoinduced electrons by the surface-deposited Ag_2O/Ag^0.

For both the reduction methods, variation in the photocatalytic activity as a function of Ag concentration is primarily governed by the corresponding variation in the amount of surface-adsorbed MB, which is in turn dependent on the variation in the surface concentration of superoxide ions. The formation of Ag_2O and SnO_2 tends to reduce the surface concentration of superoxide ions, whereas the presence of Ag^0 and Sn^{2+} ions tends to increase it. As a result of optimum balance between the effects of these parameters, the maximum photocatalytic activity ($k_{app} = 0.228$ min^{-1}) has been observed at 0.1 mol % Ag for the chemical-reduction (using Sn^{2+} ions) method.

Among the two techniques investigated for depositing Ag_2O/Ag^0 on the surface, the chemical-reduction (using Sn^{2+} ions) method appears to be more effective than the UV-reduction method to enhance the photocatalytic activity of the sol−gel derived nanocrystalline anatase TiO_2 under UV-radiation exposure.

Acknowledgment. Authors thank the Department of Science and Technology (DST), India (Project No. GAP 205139), and CSIR, India (Network Project No. NWP0010 and Task Force Project No. CMM0019), for funding the ceramic, nanotechnology, and photocatalysis research at NIIST-CSIR. Authors also thank Mr. M. R. Chandran, Mr. P. Mukundan (both from NIIST-CSIR, India), and Mr. Narendra (Icon Analytical, India) for conducting the SEM, DR, and TEM analyses respectively.

References and Notes

(1) Fujishima, A.; Rao, T. N.; Tryk, D. A. *J. Photochem. Photobiol. C* **2000**, *1*, 1.
(2) Zhang, X.; Yang, H.; Zhang, F.; Chan, K.-Y. *Mater. Lett.* **2006**, *61*, 2231.
(3) Kryukova, G. N.; Zenkovets, G. A.; Shutilov, A. A.; Wilde, M.; Gunther, K.; Fassler, D.; Richter, K. *Appl. Catal., B* **2006**, *71*, 169.
(4) Siemon, U.; Bahnemann, D.; Testa, J. J.; Rodriguez, D.; Litter, M. I.; Bruno, N. *J. Photochem. Photobiol. A* **2002**, *148*, 247.
(5) Sun, B.; Vorontsov, A. V.; Smirniotis, P. G. *Langmuir* **2003**, *19*, 3151.
(6) Arabatzis, I. M.; Stergiopoulos, T.; Andreeva, D.; Kitova, S.; Neophytides, S. G.; Falaras, P. *J. Catal.* **2003**, *220*, 127.
(7) Pal, B.; Ikeda, S.; Kominami, H.; Kera, Y.; Ohtani, B. *J. Catal.* **2003**, *217*, 152.
(8) Millard, L.; Bowker, M. *J. Photochem. Photobiol. A* **2002**, *148*, 91.
(9) Korosi, L.; Papp, S.; Menesi, J.; Illes, E.; Zollmer, V.; Richardt, A.; Dekany, I. *Colloids Surf. A* **2008**, *319*, 136.
(10) Vamathevan, V.; Amal, R.; Beydoun, D.; Low, G.; McEvoy, S. *Chem. Eng. J.* **2004**, *98*, 127.
(11) Vamathevan, V.; Amal, R.; Beydoun, D.; Low, G.; McEvoy, S. *J. Photochem. Photobiol. A* **2002**, *148*, 233.
(12) Vamathevan, V.; Tse, H.; Amal, R.; Beydoun, D.; Low, G.; McEvoy, S. *Catal. Today* **2001**, *68*, 201.
(13) Arabatzis, I. M.; Stergiopoulos, T.; Bernard, M. C.; Labou, D.; Neophytides, S. G.; Falaras, P. *Appl. Catal., B* **2003**, *42*, 187.
(14) Kuo, Y.-L.; Chen, H.-W.; Ku, Y. *Thin Solid Films* **2007**, *515*, 3461.
(15) Tan, T. T. Y.; Yip, C. K.; Beydoun, D.; Amal, R. *Chem. Eng. J.* **2003**, *95*, 179.
(16) Zhang, F.; Guan, N.; Li, Y.; Zhang, X.; Chen, J.; Zeng, H. *Langmuir* **2003**, *19*, 8230.
(17) Cozzoli, P. D.; Fanizza, E.; Comparelli, R.; Curri, M. L.; Agostiano, A.; Laub, D. *J. Phys. Chem. B* **2004**, *108*, 9623.
(18) Xu, M.-W.; Bao, S.-J.; Zhang, X.-G. *Mater. Lett.* **2005**, *59*, 2194.
(19) Chen, L.-C.; Tsai, F.-R.; Huang, C.-M. *J. Photochem. Photobiol. A* **2005**, *170*, 7.

(20) Bowering, N.; Croston, D.; Harrison, P. G.; Walker, G. S. *Int. J. Photoenergy* **2007**, Article Number 90752.
(21) Andersson, M.; Birkedal, H.; Franklin, N. R.; Ostomel, T.; Boettcher, S.; Palmqvist, A. E. C.; Stucky, G. D. *Chem. Mater.* **2005**, *17*, 1409.
(22) Ozkan, A.; Ozkan, M. H.; Gurkan, R.; Akcay, M.; Sokmen, M. *J. Photochem. Photobiol. A* **2004**, *163*, 29.
(23) Sokmen, M. Ozkan, A. *J. Photochem. Photobiol. A* **2002**, *147*, 77.
(24) Tsuji, H.; Sakai, N.; Gotoh, Y.; Ishikawa, J. *Nucl. Instrum. Methods Phys. Res. B* **2006**, *242*, 129.
(25) Tsuji, H.; Sugahara, H.; Gotoh, Y.; Ishikawa, J. *Nucl. Instrum. Methods Phys. Res. B* **2003**, *206*, 249.
(26) Zhang, F.; Jin, R.; Chen, J.; Shao, C.; Gao, W.; Li, L.; Guan, N. *J. Catal.* **2005**, *232*, 424.
(27) Shukla, S.; Seal, S.; Akesson, J.; Oder, R.; Carter, R.; Rahman, Z. *Appl. Surf. Sci.* **2001**, *181*, 35.
(28) Shukla, S.; Seal, S.; Rahman, Z.; Scammon, K. *Mater. Lett.* **2002**, *57*, 151.
(29) Baiju, K. V.; Shukla, S.; Sandhya, S.; James, J.; Warrier, K. G. K. *J. Phys. Chem. C* **2007**, *111*, 7612.
(30) Baiju, K. V.; Shukla, S.; Sandhya, S.; James, J.; Warrier, K. G. K. *J. Sol-Gel Sci. Technol.* **2008**, *45*, 165.
(31) Zachariah, A.; Baiju, K. V.; Shukla, S.; Deepa, K. S.; James, J.; Warrier, K. G. K. *J. Phys. Chem. C* **2008**, *112*, 11345.
(32) Barr, T.; Seal, S. *J. Vac. Sci. Technol. A* **1995**, *13*, 1239.
(33) Choi, T.-H.; Hong, S.-H. *Sens. Actuators B* **2007**, *125*, 504.
(34) Lin, H.; Huang, C. P.; Li, W.; Ni, C.; Shah, S. I.; Tseng, Y.-H. *Appl. Catal., B* **2006**, *68*, 1.
(35) Porkodi, K.; Arokiamary, S. D. *Mater. Charact.* **2007**, *58*, 495.
(36) Zhao, Y.; Li, C.; Liu, X.; Gu, F.; Jiang, H.; Shao, W.; Zhang, L.; He, Y. *Mater. Lett.* **2007**, *61*, 79.
(37) Liqiang, J.; Yichuhn, Q.; Baiqi, W.; Shudan, L.; Baojiang, J.; Libin, Y.; Wei, F.; Honggang, F.; Jiazhong, S. *Sol. Energy Mater. Sol. Cells* **2006**, *90*, 1773.
(38) Zhou, X. D.; Huebner, W. *Appl. Phys. Lett.* **2001**, *79*, 3512.
(39) Okumura, M.; Coronado, J. M.; Soria, J.; Haruta, M.; Conesa, J. C. *J. Catal.* **2001**, *203*, 268.
(40) Yang, X.; Xu, L.; Yu, X.; Guo, Y. *Catal. Commun.* **2008**, *9*, 1224.
(41) Shibata, S.; Aoki, K.; Yano, T.; Yamane, M. *J. Sol-Gel Sci. Technol.* **1998**, *11*, 279.
(42) Shukla, S.; Seal, S. *Nanostruct. Mater.* **1999**, *11*, 1181.
(43) Nicole, J.; Tsiplakides, D.; Pliangos, C.; Verikios, X. E.; Comninellis, Ch.; Vayenas, C. G. *J. Catal.* **2001**, *204*, 23.
(44) Yu, J.; Xiong, J.; Cheng, B.; Liu, S. *Appl. Catal., B* **2005**, *60*, 211.
(45) Houas, A.; Lachheb, H.; Ksibi, M.; Elaloui, E.; Guillard, C.; Herrmann, J.-M. *Appl. Catal., B* **2001**, *31*, 145.
(46) Senthilkumaar, S.; Porkodi, K.; Gomathi, R.; Maheswari, A. G.; Manonmani, N. *Dyes Pigm.* **2002**, *69*, 22.

JP8105343